Flows Produced by Discrete Sources of Buoyancy

MICHAEL K. DAVEY* AND PETER D. KILLWORTH**

Hooke Institute for Atmospheric Research, Department of Atmospheric, Oceanic and Planetary Physics, University of Oxford, Parks Road, Oxford, United Kingdom

(Manuscript received 22 February 1988, in final form 9 January 1989)

ABSTRACT

The response of an ocean with a single active dynamical layer (notionally with an infinitely thick upper layer above it, of slightly less density) to localized buoyancy forcing on a beta-plane is considered. It is shown that three regimes exist. When the forcing is very weak, the response is linear, and consists of a quasi-steady "tube" of fluid stretching westwards from the forcing region, with a front advancing at the long Rossby wave speed, and some transient structure in the vicinity of the forcing. When the amplitude of the forcing is increased, potential vorticity contours are sufficiently deformed to permit instability both in the forced region and to its west. The response becomes a series of shed eddies, each of which propagates westwards. The time scale to generate an eddy is proportional to the time taken for a long Rossby wave to propagate across the forced region. Further increase in forcing amplitude yields a completely unsteady response.

1. Introduction

The ocean circulation is driven by wind and buoyancy forcing, both of which act predominantly at the ocean surface. The flows produced by wind stress are relatively straightforward to model, at least when the resulting flow is sufficiently slow to obey linear dynamics. Flows produced by buoyancy forcing, however, are intrinsically nonlinear (because the mass field is altered) and much harder to understand. Thus recent studies of buoyancy driving have tended to concentrate on relatively simple systems with few degrees of freedom in the vertical; and even in such studies, the analyses rapidly become complex. The assumption is frequently made that the system—presumably forced in a time-independent manner—is in a steady state. To ensure this, the spatial scale of the forcing must be of order of the gyre scale to avoid possible instabilities which would invalidate the solutions. Talley (1979) and Luyten and Stommel (1985) have discussed steady solutions in this regime.

The work presented here was motivated by two different questions. The first arose because there are many occurrences of buoyancy forcing on much smaller scales than a full gyre: the cooling of warm core rings, "chimney formations" in the polar oceans, etc. A well-documented case is the Mediterranean outflow (Kinder and Bryden 1987), which can be considered as a fairly continuous source of saline water injected into the middepth Atlantic at a rate of approximately 10^6 m^3 s^{-1}, as a side boundary condition. Despite this continuous source, much of the evidence of Mediterranean water is visible in the eastern and western Atlantic in the form of large saline lenses, or "meddies"; cf. Armi and Zenk (1984). It is not clear how or where the continuous source of salty water is broken into discrete blobs of water. Similarly, the results of deepwinter convection, e.g., in the northwestern Mediterranean, seem to leave the area of formation rather more rapidly than one might expect from a simple geostrophic adjustment analysis with a little bottom friction added. The sparse observations (e.g., Sankey 1973) suggest that the dense water breaks up into discrete blobs on a time scale of order 1 month. Recently, Whitehead (1988, personal communication) and Linden (1988, personal communication) have conducted laboratory experiments in which a slanting bottom approximately replaces a beta-plane, and dense water is injected into the fluid from a thin nozzle. This fluid, too, breaks up into a chain of eddies.

The second question relates to previous work (Davey and Killworth 1984) in which local buoyancy forcing was used as a mechanism for forming an isolated eddy, whose motion was then studied numerically. The forcing had been turned on smoothly, and then turned off again after about 10 days. What, we wondered, would happen if the forcing were not turned off? How could the excess injected water be removed? Clearly a geostrophic adjustment process would only move the water a distance of order the local deformation radius (say

* Meteorological Office, Bracknell, Berkshire, United Kingdom.
** Deacon Laboratory of the Institute of Oceanographic Sciences, Wormley, Godalming, Surrey, United Kingdom.

Corresponding author address: Dr. M. K. Davey, Hooke Institute for Atmospheric Research, Clarendon Laboratory, Parks Road, Oxford OX1 3PU, United Kingdom.

30 km). Would the water pile up near the buoyancy source?

We use the shallow water equations, as in section 2. The nonlinearity of the general problem precludes an analytical treatment. For sufficiently weak forcing, however, a linear problem can be solved in terms of Rossby waves. The main response is a region of sheared zonal flow to the west of the forcing region, as described in section 3. For stronger forcing (i.e., strong enough to generate reversals of the potential vorticity gradient) nonlinear effects are important and numerical solutions are sought, as in sections 4 and 5. In this regime a series of discrete eddies form and propagate westward.

2. Formulation

We adopt the simplest model which can allow buoyancy forcing: a one-layer reduced gravity (g') model, with a source term in the continuity equation. The active layer is either the lower of a two-layer system, or the middle of a three-layer system at rest above and below (the Mediterranean outflow might be modeled in this way, for example).

To simplify discussion we implicitly assume that the source term is confined within horizontal dimensions of order the deformation radius (otherwise another parameter relating the spatial dimensions of the forcing to the deformation radius would be involved). If the total depth h is nondimensionalized on the undisturbed value H, Coriolis parameter $f \equiv (f_0 + \beta y)$ on its mean value f_0, time t on f_0^{-1}, axes x east and y north on the deformation radius $a = \sqrt{g'H}/f_0$, velocities u (east) and v (north) on the gravity wave speed $\sqrt{g'H}$, the equations of motion become

$$u_t + \mathbf{u}\cdot\nabla u - (1 + \epsilon y)v = -h_x \tag{2.1}$$

$$v_t + \mathbf{u}\cdot\nabla v + (1 + \epsilon y)u = -h_y \tag{2.2}$$

$$h_t + \nabla\cdot(\mathbf{u}h) = Q_0 Q(x, y). \tag{2.3}$$

Here $Q(x, y)$, of dimensional amplitude Q_{00}, represents the buoyancy forcing. Buoyancy flux in a stratified ocean occurs more properly as a source term in a density equation. In a layered system, mass continuity takes the role of a density equation; hence the source term in (2.3). This conversion tends to be taken for granted (e.g., Luyten and Stommel 1985) and is discussed in section 6.

Two parameters have appeared. The first, ϵ, occurs in $f \equiv (1 + \epsilon y)$, and measures the strength of the beta-effect:

$$\epsilon = \beta a/f_0$$

$$= \beta a^2/(g'H)^{1/2}$$

long Rossby wave speed/gravity wave speed, (2.4)

and the second measures the strength of the forcing:

$$Q_0 = Q_{00}/f_0 H. \tag{2.5}$$

We shall assume that $Q(x, y) \equiv Q(r)$ in what follows, where r is a radial coordinate, and also that Q vanishes for r greater than some value of order unity. The initial condition will simply be

$$h = 1, \quad u = v = 0, \quad t = 0. \tag{2.6}$$

Typical oceanic values of the parameters can be estimated. At 30°N, an internal wave speed of 3.13 m s^{-1} (corresponding to $H = 1000$ m, $g' = 9.8 \times 10^{-3}$ m s^{-2}, $f_0 = 7.29 \times 10^{-5}$ s^{-1}, say) gives $a \sim 43$ km and

$$\epsilon \sim 1.2 \times 10^{-2}.$$

Here Q_0 can take a variety of values depending on the type of forcing. If we imagine Q to represent a mass flux of 10^6 m^3 s^{-1} distributed over a 40 km radius, then

$$Q_0 \leqslant 4 \times 10^{-3}.$$

If, however, we model Q as a steady surface forcing of, say, 100 W m^{-2}, then

$$Q_0 \sim 10^{-4}.$$

We will see later that the response to the forcing is linear and wavelike for $Q_0 \leqslant \epsilon^2$, but nonlinear and eddylike for $Q_0 \geqslant \epsilon^2$.

3. Linear theory

a. Steady state

It is useful to first consider the effect of forcing that is sufficiently weak for nonlinear terms to be neglected, and is acting for a sufficiently long time for the flow to be steady near the forced region. The steady, linear version of the nondimensional equations (2.1)–(2.3) is

$$-fv = -\eta_x \tag{3.1a}$$

$$fu = -\eta_y \tag{3.1b}$$

$$\nabla\cdot\mathbf{u} = Q_0 Q \tag{3.1c}$$

where

$$\eta = h - 1 \tag{3.2}$$

is the depth perturbation, and

$$f = 1 + \epsilon y \tag{3.3}$$

is the Coriolis parameter.

We apply the boundary condition

$$\eta = 0 \quad \text{east of the forced region} \tag{3.4}$$

because only transient waves (which leave no steady perturbation) influence this region. Then (3.1) can be solved to obtain

$$\eta(x, y) = (Q_0/\epsilon) f^2 \int_x^\infty Q(x', y)\,dx' \tag{3.5}$$

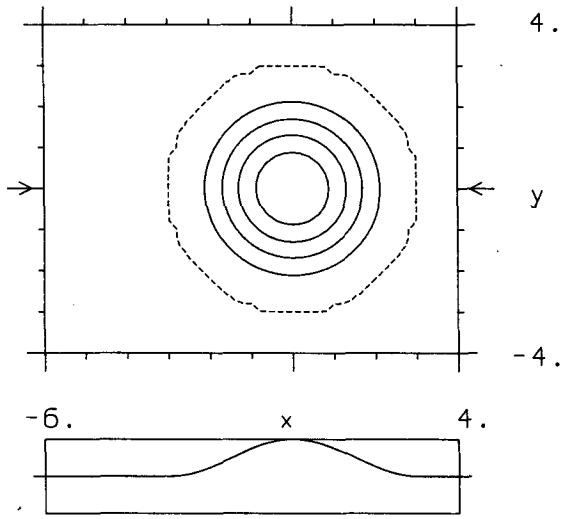

FIG. 1. Contours of the forcing $Q = \frac{1}{2}[1 + \cos(\pi r/r_0)]$ (for $r < r_0$, 0 otherwise), for $r_0 = 3$. The zero contour is dashed.

$$u(x, y) = -(Q_0/\epsilon)[f^2 \int_x^\infty Q_y(x', y)dx' + 2\epsilon \int_x^\infty Q(x', y)dx'] \quad (3.6)$$

$$v(x, y) = -(Q_0/\epsilon)fQ. \quad (3.7)$$

Several features are apparent.

(i) The response at any point depends only on the forcing directly east of that point.

(ii) When the scale of the forced region is O(1), the integrals are O(1), so η, u, and v are $O(Q_0/\epsilon)$. The reason for this scaling is that the long, westward propagating Rossby waves that determine the steady state travel at a (nondimensional) speed ϵ, taking a time $O(1/\epsilon)$ to cross the forced region and allowing a response $O(Q_0/\epsilon)$ to build up. Thus our assumption of small amplitude requires $Q_0 \ll \epsilon$ at most. (A further restriction will be imposed below.)

(iii) Nonzero velocities are found only in the forced region or directly west of it, and purely zonal flow is outside the forced region.

(iv) The meridional flow in the forced region is equatorward where $Q > 0$ (mass input), and vice versa. This meridional flow advects planetary potential vorticity at a rate just sufficient to balance generation of potential vorticity by the forcing.

To illustrate these results, we use a circular mass source with radius r_0 and distribution:

$$Q = \begin{cases} \frac{1}{2}[1 + \cos(\pi r/r_0)], & r < r_0 \\ 0, & r > r_0 \end{cases} \quad (3.8)$$

as shown in Fig. 1 with $r_0 = 3$. The steady surface displacement and the horizontal velocity (u, v) are shown in Fig. 2, scaled by (Q_0/ϵ). A "tube" of fluid can be seen stretching westward from the forced region. There is eastward flow in the northern half of the tube, and slightly larger (due to smaller f) westward flow in the southern portion, linked by flow through the forced region. The horizontal flow is slightly divergent in the forced region to accommodate the steady mass source.

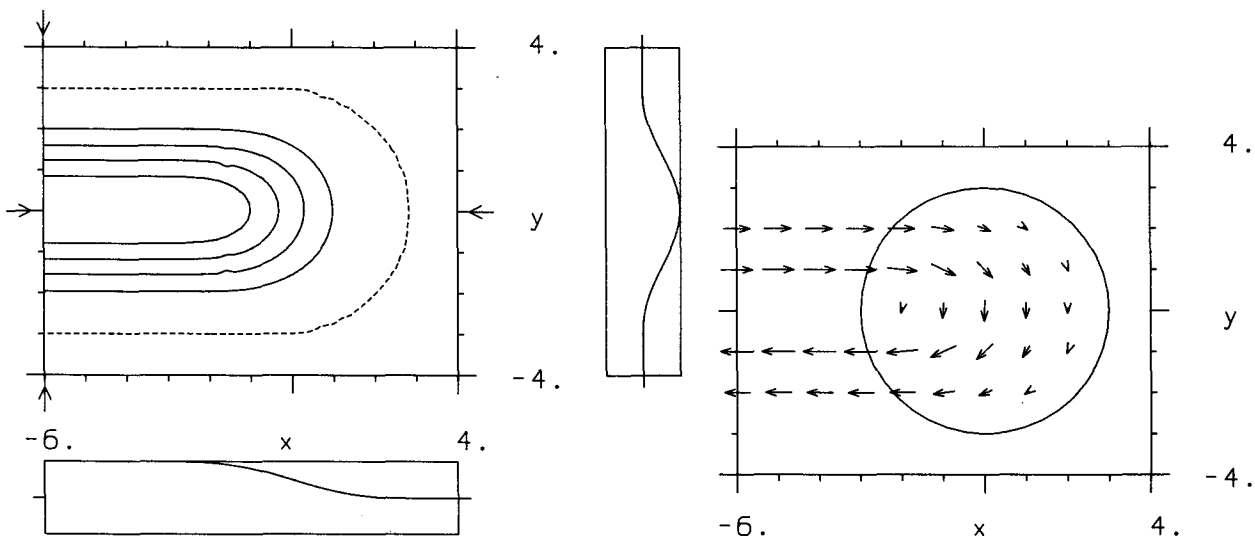

FIG. 2. Steady linear response to the forcing in Fig. 1. (a) surface displacement $\eta/(Q_0/\epsilon)$, max = 3, contour interval (ci) = 0.5. The zero contour is dashed. Arrows indicate the positions of the cross sections shown at the right of and below the contour map. The range of the cross-section plots is −max to +max. (b) horizontal velocity vectors $(u, v)/(Q_0/\epsilon)$.

b. Potential vorticity and stability

The full potential vorticity (nondimensional) in the shallow-water system is

$$q = (f + \xi)/h - 1 \tag{3.9}$$

where

$$\xi = v_x - u_y.$$

For small disturbances,

$$q \approx \epsilon y + \xi - \eta. \tag{3.10}$$

From (3.5) and (3.6), west of the forced region the meridional gradient of q is, neglecting terms $O(Q_0)$,

$$q_y \approx \epsilon + \frac{Q_0}{\epsilon}\int_x^\infty (Q_{yyy} - Q_y)dx'. \tag{3.11}$$

In the tube to the west of the forced region, q_y could change sign when $Q_0 \sim \epsilon^2$, in which case we might expect the tube to be unstable to small perturbations. (In a parallel shear flow the Rayleigh theorem guarantees stability as long as q_y does *not* change sign.)

As an example, Fig. 3 shows the term

$$I = \int_{-\infty}^{\infty} (Q_{yyy} - Q_y)dx',$$

for the forcing (3.8). This profile (which is realized west of the forced region) has a maximum value of about 4. In this case q would change sign when

$$|Q_0/\epsilon^2| \geq 0.25,$$

with the reversal occurring in the southern portion of the tube when $Q_0 > 0$.

The response to the forcing initially increases fastest in the forced region. If q_y is going to change sign, it will first do so somewhere *within* the forced region. Thus we might expect instabilities to develop in that region, and perhaps be so dominant as to prevent the tube forming to the west. The numerical results in section 5 show that this is indeed the case. To obtain the steady tube described above, we require $Q_0 \leq \epsilon^2$, which is a more severe constraint than the "small amplitude" restriction $Q_0 < \epsilon$ found earlier and required for, e.g., $\eta \ll 1$.

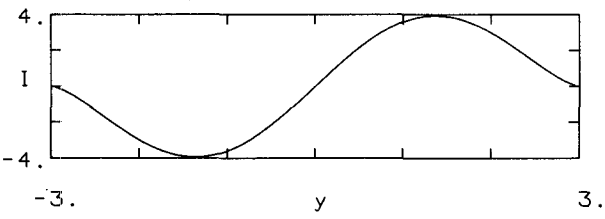

FIG. 3. The integral $I = \int_{-\infty}^{\infty} (Q_{yyy} - Q_y)dx'$ is a measure of the nonplanetary component of the meridional potential vorticity gradient west of the forced region.

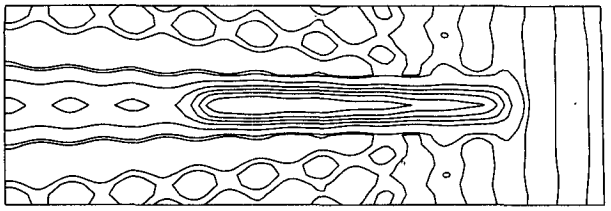

FIG. 4. The transient linear solution for surface displacement $\eta/(Q_0/\epsilon)$, as given by (A18) with $Q_0 = -3.1 \times 10^{-5}$, $\epsilon = 0.012$, forcing as in (A19) with $r_0 = 1.7$, [mimicking (3.8)] at 400 days. Max = 1.14×10^{-2}, ci = 1.7×10^{-3}. Geometry and forcing position as in Fig. 5.

c. Transient response

Before describing the nonlinear numerical results, we briefly consider the linear transient problem. On eliminating u and v, neglecting terms $\partial^2/\partial t^2$ relative to f^2, and replacing f by 1 (unless differentiated), an equation for the surface displacement η alone can be obtained:

$$\eta_t - \epsilon\eta_x - \nabla^2\eta_t = Q_0 Q. \tag{3.12}$$

(This is simply a form of the quasi-geostrophic vorticity equation.) When the term $\nabla^2\eta_t$ is omitted, only long Rossby waves are left and the solution is simply

$$\eta(x, y, t) = (Q_0/\epsilon)\int_x^{x+\epsilon t} Q(x', y)dx' \tag{3.13}$$

which tends smoothly to the steady solution (3.5) as $t \to \infty$, with f replaced by 1. (Recall that ϵ is the long Rossby wave speed, so the range of integration simply reflects the distance travelled by such waves in time t.)

The short Rossby waves allowed by (3.12) simply add further transient structures which only play a minor role. These are analyzed further in the Appendix. Figure 4 shows the approximate solution (A18) of (3.12) with forcing of the form (A19), with $Q_0 = 3.1 \times 10^{-6}$, and $\epsilon = 0.012$, at day 400 (using dimensional terms for convenience). The value of r_0 was 1.7, chosen to mimic the forcing (3.8) to a very good approximation. The solution may be compared with the numerical solution of Fig. 6 (cf. section 5). Although formally valid only near the forcing region, the behavior of the two sets of transients is clearly visible in the numerical solutions.

4. Numerical model description

To obtain solutions when nonlinear effects are important, numerical experiments were carried out by time-stepping (leapfrog) the nonlinear shallow water equations (2.1)–(2.3) on a horizontal C-grid with spacing of half a Rossby radius in the x and y directions. There are free-slip north and south sidewalls located at ten Rossby radii from the center of the forced region, and the system is zonally periodic with length 60 Rossby radii. No explicit diffusion or damping is included.

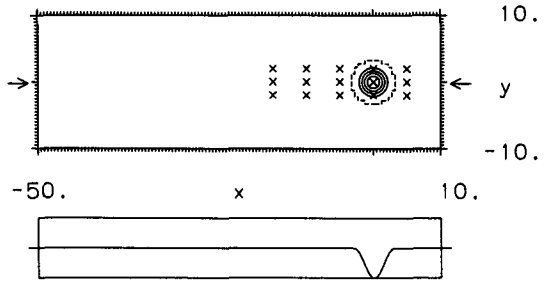

FIG. 5. The geometry and contours of the forcing pattern Q for the numerical experiments. The tick marks correspond to the horizontal grid with spacing of half a Rossby radius. Crosses mark the initial positions of passive tracers. Arrows indicate the position of the cross section shown below, which has range −max to +max.

The Coriolis parameters f_0 and β take values at 30°N. The dimensional values $g' = g/1000$ m s^{-2} and $H = 1000$ m give $\sqrt{g'H} = 3.13$ m s^{-2} and a Rossby radius of 43 km. Hence we have

$$\epsilon = (\text{long Rossby wave speed})/(g'H)^{1/2} = 0.012. \quad (4.1)$$

A mass source or sink of shape (3.8) was used. The nondimensional value for the first experiment is

$$Q_0 = -3.1 \times 10^{-5},$$

which corresponds to a dimensional value

$$Q_{00} = -0.2 \text{ m day}^{-1}.$$

Figure 5 shows the geometry and the location of the forcing, along with the initial positions of several passive tracers. To give the reader a realistic sense for the timing of events, results are described in terms of days rather than nondimensional units.

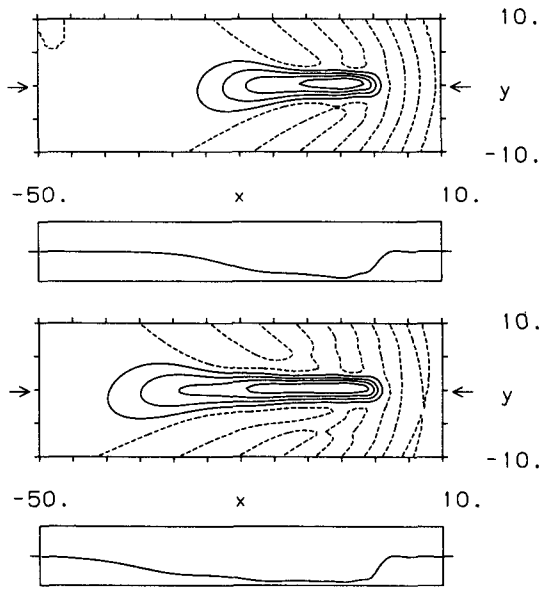

FIG. 6. Case 1: $Q_0 = -3.1 \times 10^{-5}$, $\epsilon = 0.012$. Surface displacement at (a) day 400, with max = 1.4×10^{-3}, min = -8.6×10^{-3}. (b) day 600, with max = 1.4×10^{-3}, min = -8.4×10^{-3}. Scale of cross sections is min to −min. Zero contour dashed, ci = −min/5.

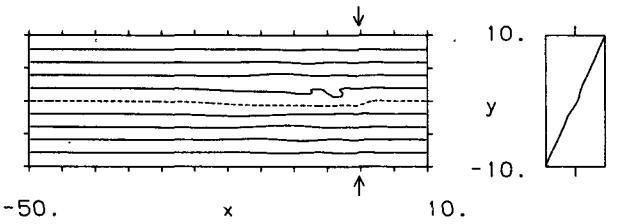

FIG. 7. Case 1: Potential vorticity q at day 400 with max = 10ϵ, min = -10ϵ, ci = 2ϵ. Zero contour dashed. Range of cross sections is −max to +max.

5. Numerical results

a. Case 1: $Q_0 < \epsilon^2$

For this first experiment we use $Q_0 = -3.1 \times 10^{-5}$, (a water mass sink) so $|Q_0/\epsilon^2| = 0.2$, which is close to the value 0.25 predicted for instability.

The surface displacement at days 400 and 600 is shown in Fig. 6. As predicted by linear theory, a tube spreads to the west of the forced region. Comparing Fig. 6a with Fig. 4 shows that the transient solution (A18) is a good approximation for this case.

Potential vorticity, as defined by (3.7), is shown in Fig. 7 for day 400. The picture is dominated by the undisturbed value ϵy. The main disturbance appears just to the west of the forced region, slightly north of the central latitude $y = 0$, where contours of q are being "wound up" by the cyclonic flow. This wind-up is just sufficient for the meridional gradient of q to reverse in a small area: too small to be dynamically significant for the flow as a whole. The response to the forcing is essentially wavelike.

Tracer movements for day 400 to 600 are given in Fig. 8. Displacements in this time are significant (typically about four Rossby radii), and predominantly zonal west of the forced region. The velocity field is very like that in Fig. 2b for the linear steady case (remember that $Q_0 < 0$ here). Vertical velocity is negligible outside the forced region.

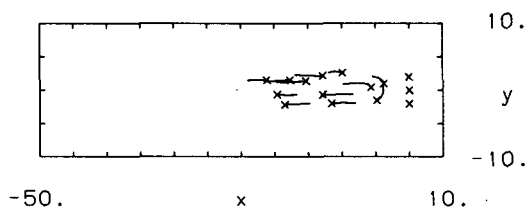

FIG. 8. Case 1: tracer movement from day 400 to day 600. See Fig. 5 for initial positions.

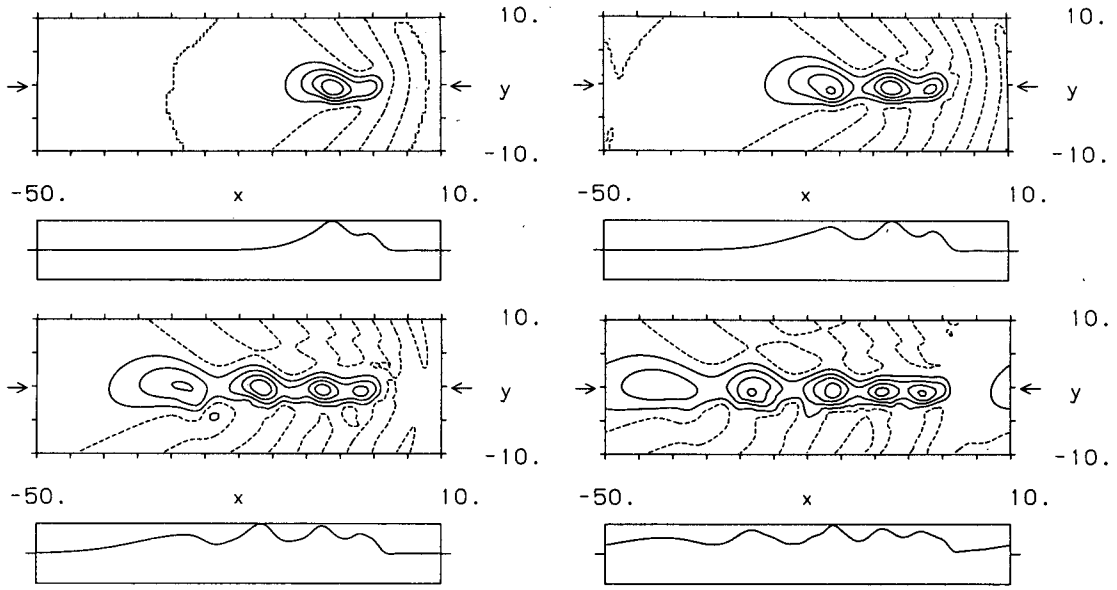

FIG. 9. Case 2: $Q_0 = 1.5 \times 10^{-4}$, $\epsilon = 0.012$. Surface displacement at (a) day 200, with max = 0.043, min = −0.004. (b) day 400, with max = 0.046, min = −0.006. (c) day 600, with max = 0.049, min = −0.011. (d) day 800, with max = 0.048, min = −0.010. Zero contour dashed, ci = max/5.

Changing the sign of Q (a water mass source rather than sink) leads to very nearly the same response, with the sign of u, v and η reversed. As the amplitude of Q_0 is reduced the pattern remains the same, with tracer movements reduced proportionally and less displacement of the basic potential vorticity pattern.

b. *Case 2: $Q_0 > \epsilon^2$*

Increasing the amplitude of the forcing by a factor of 5 to $Q_0 = 1.5 \times 10^{-5}$ (so $Q_0/\epsilon^2 \approx 1$, but $Q_0/\epsilon \ll 1$) leads to rather different behavior.

A sequence of maps of the surface displacement is

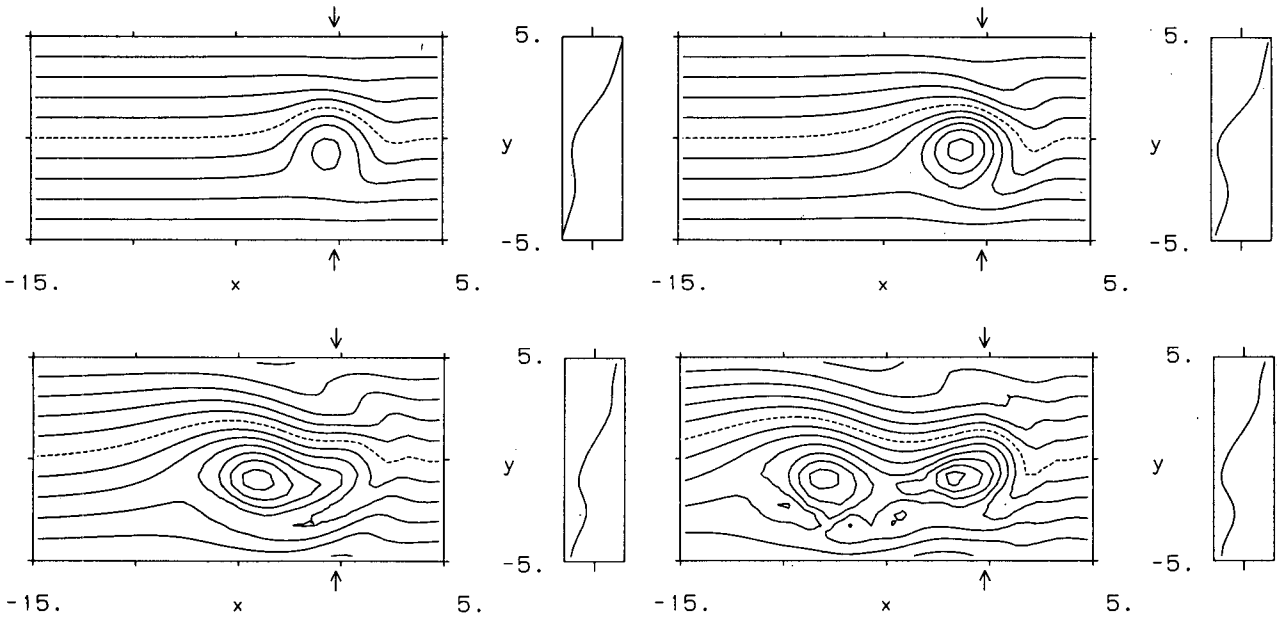

FIG. 10. Case 2: potential vorticity q in and near the forced region [a circle of radius 3, centered on (0, 0)]. Zero contour dashed, contour interval ϵ. (a) day 40, (b) day 80, (c) day 160, (d) day 240.

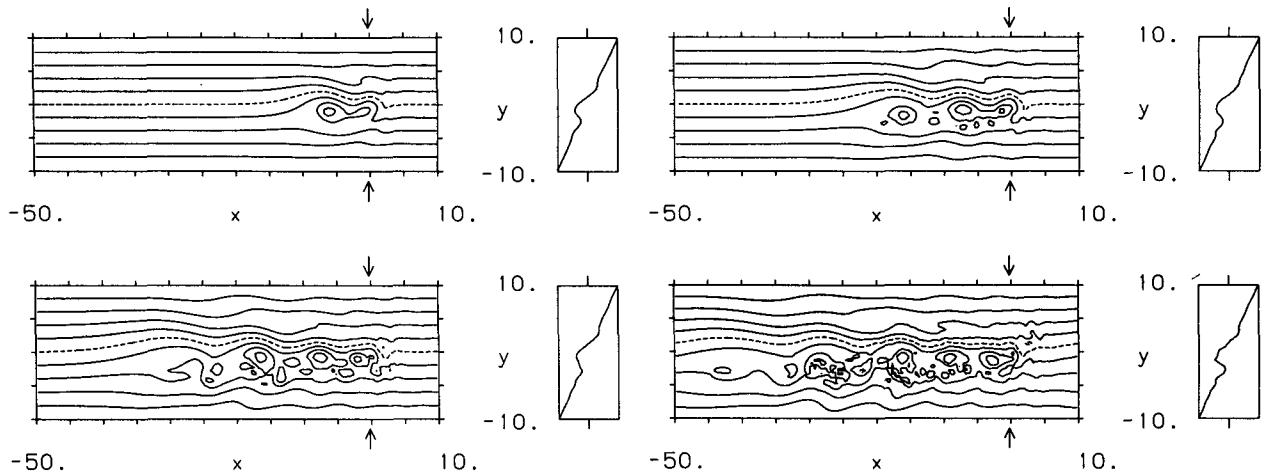

FIG. 11. Case 2: potential vorticity q, with max = 10ϵ, min = -10ϵ, ci = 2ϵ. Zero contour dashed. (a) day 200, (b) day 400, (c) day 600, (d) day 800.

given in Fig. 9, for days 200, 400, 600 and 800. At day 200 the disturbance is spreading west as before, but now the maximum is clearly west of the forced region. By day 400 there are two distinct eddies, and a third seems to be forming in the forced region. By day 600 there are three eddies in a line west of the forced region, with four at day 800. Rather than a tube, we have a series of blobs.

The detailed potential vorticity maps in Fig. 10 show more clearly how these eddies are forming. The mass source tends to decrease the potential vorticity q, and by day 40 (Fig. 10a) the change is large enough for a region of closed q-contours to appear, with its center located south of the forcing maximum. (This offset is due to the gradient of planetary vorticity: for a mass sink the q-center would be north of the forcing maximum.) By day 80 this closed region, marking an eddy, has strengthened and the center has moved westward to the edge of the forced region. The anticyclonic circulation advects potential vorticity around the eddy, tending to increase q on its eastern side, as indicated by the wraparound effect in Fig. 10b. Importantly, this advection of q opposes the decrease due to the mass source. By day 160 the eddy has propagated further west, clear of the forced region. Advection has suppressed the further formation of water with q as low as that in the eddy, so the eddy is distinct. Potential vorticity is conserved outside the forced region, and thus acts as a tracer, so the westward movement of closed q-contours indicates the material transport of fluid.

As the eddy moves further away from the forced region the advection effect weakens and the forcing again generates low q, forming another eddy. Thus in Fig. 10d at day 240 there are two separate regions of low q: one is the original eddy still propagating west, and the second is the next eddy beginning to move out of the forced region (cf. Fig. 10b). The process repeats, with a new eddy forming at intervals of about 160 days. Figure 11 shows the q-field for the same area and times as for the height fields in Fig. 9: the blobs in Fig. 9 can be identified with the closed regions of low q. The eddies appear to break up after moving about 40 Rossby radii west, but whether this is due to eddy interactions, current shear, or numerical effects is unclear.

Several tracer tracks are shown in Fig. 12. Figure 12a (day 0 to 200) contains the looping trajectory of the tracer that started at the center of the forced region. This tracer then follows a cusped track westward until day 600 (it is the westernmost tracer in Fig. 12c, at day 600). It then travels southwest (Fig. 12d) as the eddy containing it is absorbed into its surroundings.

Figure 12a shows the rapid movement of the tracer near the forced region, with substantial northward movement by the group to the west. Such meridional movement contrasts with the gentler, mainly zonal flow induced by weaker forcing. The q-field is considerably distorted, and the dynamics become highly nonlinear as eddies form and interact. Note that there is very little movement east of the forced region. (The tracer movement here in Fig. 12d is due to the east–west periodicity of the model.)

The velocity components at day 800 can be seen in Fig. 13. The zonal flow is east toward the forced region ($Q > 0$) for $y > 0$, and erratic and mainly westward for $y < 0$. Meridional flow is strong (amplitude comparable with u), even far west of the forced region, with alternating northward and southward direction reflecting the sequence of distinct eddies. Maximum flow speed is seven times greater than the long Rossby wave speed. There is strong convergence and divergence associated with the eddies, as seen in the vertical velocity map in Fig. 13c. This contrasts with the more weakly forced case, for which vertical velocity was virtually zero outside the forced region.

The eddies move westwards at around 82% of the

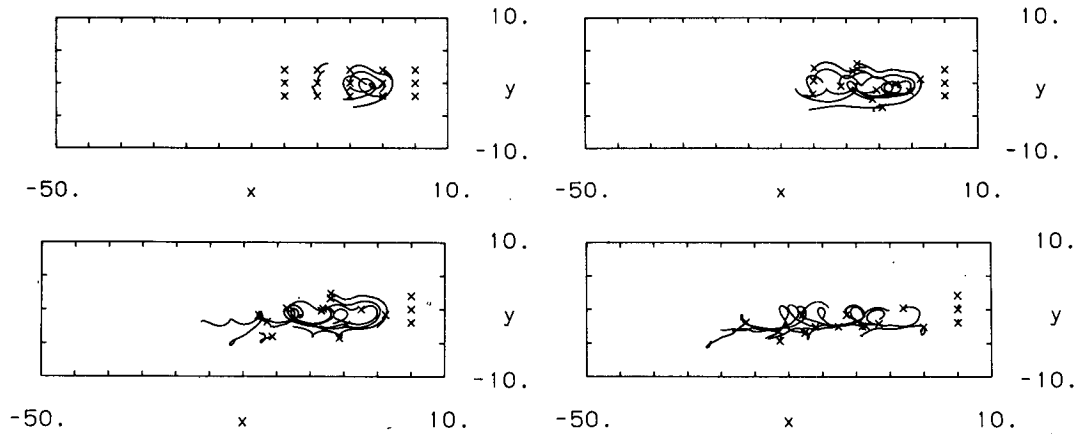

FIG. 12. Case 2: tracer trajectories, with positions at the start of each interval marked by a cross. (a) day 0–200, (b) day 200–400, (c) day 400–600, (d) day 600–800.

long Rossby wave speed. At first sight this may seem puzzling. Davey and Killworth (1984) showed that anticyclonic eddies in this system which were approximately radially symmetric traveled faster than the long-wave speed. It is possible to extend their arguments to show that all anticyclones in a one-layer system move westwards faster than the long-wave speed (appendix B). How, then, do our solutions move slower than the long-wave speed? A solution can be found in appendix B, which shows that a chain of eddies, connected by "tails" like those in Fig. 9, are retarded by interactions between the eddies.

It is also tempting to wonder whether some of the observed eddy structure is due to instability of the tube of fluid extending westwards. Provided $Q_0 > \epsilon^2$, this tube is indeed unstable to infinitesimal perturbations. (These cannot be fully baroclinic, because of the absence of a second, active, layer.) Straightforward linear instability calculations were performed for forcing of the form (3.8), which specifies the fields in the tube by (3.5) and (3.6). Their details are not presented here. The results showed that over a decade of Q_0 values (2×10^{-4} to 3×10^{-3}), the wavelength of maximum growth was very uniform at 7.8 deformation radii, which is a little smaller than the observed eddy spacing of around 10 deformation radii. The phase speed, however, varied between 43% and 73% of the long-wave speed, rather slower than the observed value of 82%. Thus the eddy structure seen numerically is unlikely to be produced by local instability.

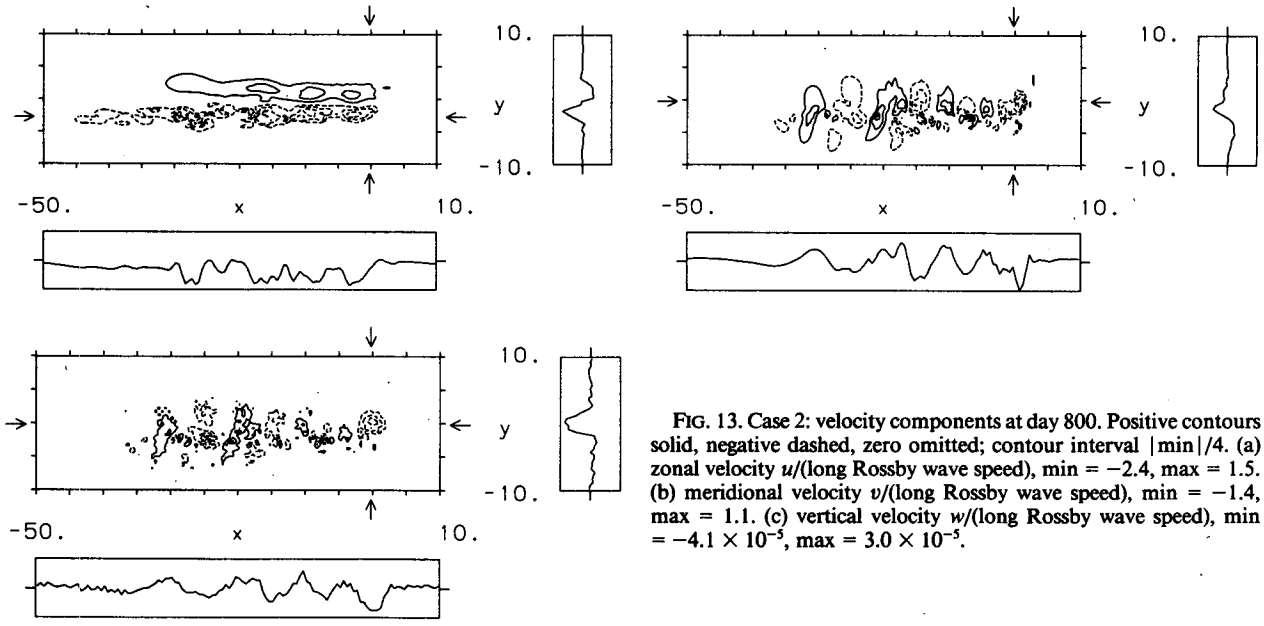

FIG. 13. Case 2: velocity components at day 800. Positive contours solid, negative dashed, zero omitted; contour interval |min|/4. (a) zonal velocity u/(long Rossby wave speed), min = −2.4, max = 1.5. (b) meridional velocity v/(long Rossby wave speed), min = −1.4, max = 1.1. (c) vertical velocity w/(long Rossby wave speed), min = -4.1×10^{-5}, max = 3.0×10^{-5}.

c. *Other cases with eddies*

Source and sink experiments with double the forcing strength used in case 1 led to the formation of a string of very small eddies in the q-field. These were too weak to perturb the system substantially, and the overall picture was still linear and wavelike, with mainly zonal currents west of the forced region. The eddies were carried westward by these currents, being located north of $y = 0$ for $Q_0 < 0$, and south of $y = 0$ for $Q_0 > 0$.

An experiment with double the forcing used in case 2 was also carried out, with qualitatively the same result. Larger eddies formed, with little difference in rate of formation, and traveled westward about 20% faster than in case 2. Motion was more vigorous and more erratic, with small scale features appearing that were undoubtedly affected by the finite resolution of the numerical model.

In another experiment with the same forcing amplitude as in case 2, but spread over a region twice as wide, the rate of eddy formation was halved. The individual eddies propagated westward at about the long Rossby wave speed. On doubling the forcing amplitude in this case, the rate of eddy formation was essentially unchanged.

d. *The mechanism of eddy formation*

From the numerical experiments, two features of the generation of distinct eddies are that (i) the timescale is effectively independent of the forcing amplitude, and (ii) the timescale is proportional to the forcing length scale. An explanation of these features can be based on the time for an eddy to propagate out of the forced region, as follows.

Suppose the forcing has length scale r_0 and amplitude Q_0. Similarly to the analysis in section 3, the surface displacement anomaly $Q_0 r_0/\epsilon$ and the velocity scale $V = Q_0/\epsilon$ initially established in the forced region are determined by the time r_0/ϵ for a long Rossby wave to travel a distance r_0. Meridional advection of potential vorticity into the center of the forced region is approximately $V\epsilon = Q_0$, sufficient to balance the effect of the forcing itself. This is true regardless of whether a region of closed q-contours has formed, and regardless of the forcing amplitude. If such a region does appear, it travels westward at about a speed ϵ, but its size is limited by the balance of q advection and forcing in the generation region, giving rise to a distinct eddy.

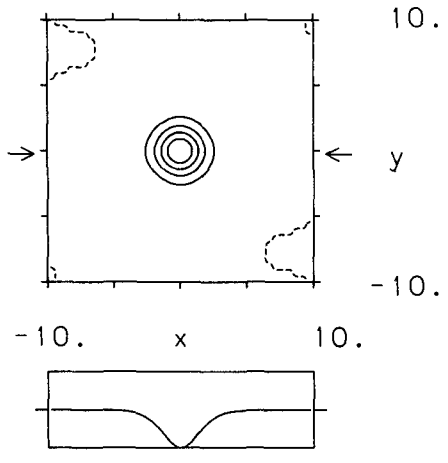

FIG. 14. The f-plane experiment: $Q_0 = -3.1 \times 10^{-3}$, $\epsilon = 0$. Surface displacement at day 50, with min = −0.62, max = 1.4×10^{-4}. Negative contours solid, zero dashed.

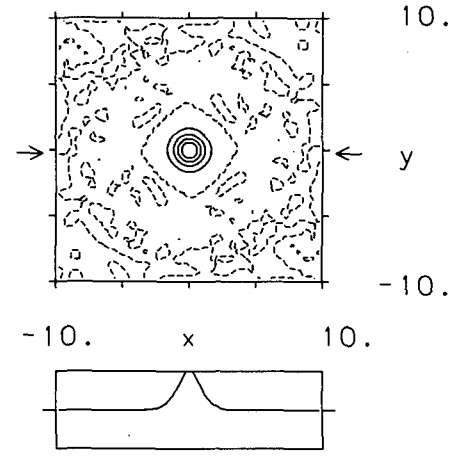

FIG. 15. The f-plane experiment: potential vorticity at day 50, with min = −0.074, max = 3.0. Positive contours solid, zero dashed.

As the eddy moves westward as a separate entity (at a speed comparable to the long Rossby wave speed), so does the circulation induced around it, and thus the velocity in the forced region weakens. After a time of order r_0/ϵ, advection in the forced region is weak enough for the forcing to generate the next eddy.

This sequence of events is consistent with the numerical results; in each case the timescale for eddy formation and shedding is about $4r_0/\epsilon$. Instability that may occur due to the reversal of potential vorticity gradients does not seem to be a factor in the eddy generation, though it may affect the subsequent evolution of a train of eddies.

e. *An f-plane experiment*

On a beta-plane disturbances tend to travel west out of the forced region, thereby limiting the amplitude of the response. On an f-plane this self-limiting mechanism is not available, and the disturbance can continue to increase.

An experiment was carried out with $\epsilon = 0$ and with very strong forcing $Q_0 = -3.1 \times 10^{-3}$. Figure 14 shows the surface displacement at day 50: the pattern is circular, with minimum value −0.62. The central depth has already reduced to 38% of its original value! The geometry and numerical grid introduce small asymmetries, as can be seen in the potential vorticity map

in Fig. 15; apparently the circular flow is stable to such perturbations. The flow and the potential vorticity contours are almost aligned, so there is no significant distortion of the q-field by advection. The numerical model was not designed to cope with vanishing depth, so this experiment ended abruptly.

6. Discussion

Numerical experiments using the inviscid nonlinear shallow water equations have shown that a sufficiently strong constant buoyancy source will generate a string of discrete eddies, marked by closed potential vorticity contours. The eddies form successively in the forced region and propagate westward. By contrast, a weak source produces a linear Rossby wave response in the form of a tube extending westward from the source.

From simple analysis, we estimate that eddies form when the forcing is strong enough to generate closed contours of potential vorticity. This occurs when $|Q_0|$ is larger than ϵ^2, where $Q_0 = Q_{00}/f_0H$ is a nondimensional measure of the source strength, and ϵ is the ratio of baroclinic long Rossby and gravity wave speeds. This criterion also depends on the shape of the source.

By this measure, eddy formation requires deepening (or shallowing) of the fluid layer of interest at a rate $Q_{00} \sim \epsilon^2 f_0 H$, where H is the depth scale of the layer. Typical midlatitude values require $Q_{00} \sim 10^{-8} H$ m s^{-1} $\sim 10^{-3} H$ m day^{-1}. A source can be expected to adjust geostrophically to a horizontal scale like the Rossby radius. For a circular source of radius 40 km, the volume flux needed for instability and eddy formation is larger than about $10^4 H$ m^3 s^{-1}.

The source could be a direct volume flux (such as the Mediterranean outflow), or indirectly caused by, for example, surface cooling. The cooling rate needed to change water density by $\Delta\rho$ to supply a source of strength Q_{00} is $(\Delta\rho c_P/\alpha)Q_{00}$, where α is the coefficient of thermal expansion. For $\Delta\rho/\rho = 10^{-3}$, $c_P = 4 \times 10^3$ J kg^{-1} °K^{-1}, $\alpha = 2.5 \times 10^{-4}$ °K^{-1}, the cooling needed for eddy formation by this mechanism in a layer of depth 1000 m is about 200 W m^{-2}. In practice, we envision the source to have a relatively small area (Killworth 1983) feeding into a deeper layer, so intense cooling would be required to supply a distributed source sufficiently strong for eddy formation.

To form the first of a train of eddies, the source must operate for a time greater than the ratio of the length scale of the source to the long Rossby wave speed. For a length scale of 100 km and wave speed 0.03 m s^{-1}, this time is of order 30 days. When the eddy first forms, advection of potential vorticity counteracts the forcing, so continued generation of anomalous potential vorticity is suppressed. Once the eddy has moved away from the forced region, advection weakens and a new eddy begins to form in the forced region. Thus this timescale is also the timescale for the rate of formation of eddies.

These experiments with a single active layer are limited by the simple density structure and the need to have an idealized mass source for the forcing. Further work with multiple layers or levels is needed to explore this eddy generation mechanism more thoroughly.

APPENDIX A

The Transient Linear Solution

We wish to solve the quasi-geostrophic governing equation (3.12). If the forcing $Q(x, y)$ is represented by a Fourier decomposition,

$$Q = \int_{-\infty}^{\infty}\int dkdmQ'(k, m) \exp[i(kx + my)], \quad \text{(A1)}$$

where Q' is given by

$$Q' = (1/4\pi^2) \int_{-\infty}^{\infty}\int dxdyQ(x, y) \exp[-i(kx + my)]. \quad \text{(A2)}$$

Then

$$\eta(x, y, t) = (iQ_0/\epsilon) \int_{-\infty}^{\infty}\int dkdm(Q'/k) \times \exp[i(kx + my)]\{A + B\} \quad \text{(A3)}$$

where

$$A = 1 - \exp(i\epsilon kt) \quad \text{(A4)}$$

$$B = \exp(i\epsilon kt) - \exp[i\epsilon kt/(1 + k^2 + m^2)]. \quad \text{(A5)}$$

The term involving A merely yields the long Rossby wave solution (3.13), and need not be considered further. (It also contains the area average of the solution, permitting what follows.) The term in B contains the transient short Rossby waves, and can be simplified for large times following the stationary phase methods of Longuet-Higgins (1965).

We put

$$X = x/\epsilon t, \quad Y = y/\epsilon t \quad \text{(A6)}$$

and seek the values of (k, m) that give stationary phase in either expression in (A5). The first term has no stationary points, but the second {after multiplication by $\exp[i(kx + my)]$} becomes

$$\exp\{it[kX + mY + \epsilon k/(1 + k^2 + m^2)]\} \quad \text{(A7)}$$

which is stationary when

$$X + (1 + m^2 - k^2)/(1 + k^2 + m^2)^2 = 0$$
$$Y - 2km/(1 + k^2 + m^2)^2 = 0 \quad \text{(A8)}$$

which are the points with zero group velocity (the long and short planetary waves). Near such points, the integral of (A7) becomes approximately (cf. Longuet-Higgins 1965)

$$\pm 2\pi/(i\Delta^{1/2}t), \quad \text{for} \quad \Delta > 0, \quad \text{according as} \quad \sigma_{kk} > 0 \text{ or } <0$$
$$2\pi/[(-\Delta)^{1/2}t], \quad \text{for} \quad \Delta < 0 \qquad \text{(A9)}$$

where we first define $\sigma = -\epsilon k/(1 + k^2 + m^2)$, and put

$$\Delta = \sigma_{kk}\sigma_{mm} - \sigma_{km}^2 = 4\epsilon^2[(3k^2 - m^2) - (k^2 + m^2)^2]/(1 + k^2 + m^2)^5. \qquad \text{(A10)}$$

Longuet-Higgins terms the solutions with positive Δ transverse waves, and those with negative Δ longitudinal waves, a practice followed here.

There are two solutions for positive Δ: $k = \pm k_1$, $m = \pm m_1$. These combine, with all the other factors, to give a contribution to η of

$$-4\pi Q_0 Q'(k_1, m_1) \cos(k_1 x + m_1 y + \epsilon k_1 t/(1 + {k_1}^2 + {m_1}^2))/\epsilon t k_1 {\Delta_1}^{1/2} \qquad \text{(A11)}$$

where

$$|{\Delta_1}^{1/2}| = 2\epsilon|3{k_1}^2 - {m_1}^2 - ({k_1}^2 + {m_1}^2)^2|^{1/2}/(1 + {k_1}^2 + {m_1}^2)^{5/2} \qquad \text{(A12)}$$

while the solutions for negative Δ ($k = \pm k_2$, $m = \pm m_2$) give

$$4\pi Q_0 Q'(k_2, m_2) \sin(k_2 x + m_2 y + \epsilon k_2 t/(1 + k_2^2 + m_2^2)/\epsilon t k_2 |\Delta_2|^{1/2}. \qquad \text{(A13)}$$

Since we are interested in the solution near the forcing region, we consider $(X, Y) \to 0$. Pair 1 now becomes $k = \pm 1$, $m = 0$, with $\Delta^{1/2} = \epsilon/2$. (A13) then simplifies to

$$-8\pi Q_0 Q'(1, 0) \cos(x + \epsilon t/2)/\epsilon^2 t. \qquad \text{(A14)}$$

This demonstrates a westward propagating wave at half the long-wave speed. Pair 2 is more subtle, as Longuet-Higgins shows. If we define

$$R = \epsilon t x = \epsilon^2 t^2 X$$
$$S = \epsilon t y = \epsilon^2 t^2 Y \qquad \text{(A15)}$$

and then define

$$p = \sqrt{R^2 + S^2}$$
$$q = R + p, \qquad \text{(A16)}$$

then the pair 2 contribution becomes, in total,

$$2^{3/2}\pi Q_0 t Q'(\epsilon t/p^{1/2}) \sin[\sqrt{(2q)}]/\sqrt{(pq)}, \qquad \text{(A17)}$$

where we have assumed Q to be radially symmetric, so that $Q'(k, m) = Q'[(k^2 + m^2)^{1/2}]$. Thus the solution for η for long times, near the origin, is

$$\eta \sim (Q_0/\epsilon)\left\{\int_x^{x+\epsilon t} Q(x', y)dx' - 8\pi Q'(1)\cos(x + \epsilon t/2)/\epsilon t + 2^{3/2}\pi\epsilon t Q'(\epsilon t/p^{1/2}) \sin(\sqrt{2q})/\sqrt{pq}\right\}. \qquad \text{(A18)}$$

Here the terms are, respectively, the long-wave, transverse, and longitudinal solutions.

For a Gaussian forcing, for example,

$$Q = \exp[-(r/r_0)^2], \qquad \text{(A19)}$$

we have

$$Q'(K) = r_0^2 \exp[-(K^2 r_0^2/4)]/4\pi, \qquad \text{(A20)}$$

and it is straightforward to evaluate (A18) and compare it with direct solutions. Figure 4 shows that the agreement is quite good in the neighborhood of the origin, as required.

APPENDIX B

Speed of Propagation of the Center of Mass of the Eddies in Case 2

Davey and Killworth (1984) used an extension of the Ball (1963) arguments to examine the propagation speed of eddies, concentrating on radially symmetric solutions. We here extend their arguments to include general (i.e. nonsymmetric) height distributions, and also include the effect on the propagation speed of a chain of eddies.

a. General shape

We have, from Davey and Killworth, that the x-propagation speed is

$$X_t = -\epsilon \iint y\bar{h}u dA/M, \qquad \text{(B1)}$$

where the integral is taken over an area A bounded by $h \to 1$, and M is the mass anomaly

$$M = \iint (h - 1)dA. \qquad \text{(B2)}$$

When ϵ is small, the values of h and u can be taken approximately as the leading order (f-plane) solutions of the steady momentum and mass balance equations (2.1)–(2.3), since X_t is automatically small because of the ϵ factor. To evaluate (B1), multiply (2.2) by yh, with time derivatives and ϵ set to zero, and integrate over A:

$$\iint yh(uv_x + vv_y)dA + \iint yhudA = -\iint yhh_y dA = \frac{1}{2}\iint (h^2 - 1)dA \qquad \text{(B3)}$$

after integration by parts. The first two terms can also be integrated by parts, and after use of the steady version of (2.3), yield

$$\iint yhudA = \iint \left[\frac{1}{2}(h^2 - 1) + hv^2\right]dA \quad \text{(B4)}$$

and so

$$X_t = -\epsilon \iint \left[\frac{1}{2}(h^2 - 1) + hv^2\right]dA/M = -\epsilon E/M \quad \text{(B5)}$$

which can be compared with Davey and Killworth's (4.7b); note that v, but not u, occurs in the definition of E.

For an anticyclone ($h \geqslant 1$),

$$\frac{1}{2}(h^2 - 1) + hv^2 > \frac{1}{2}(h^2 - 1) > (h - 1) \quad \text{(B6)}$$

so that

$$X_t < -\epsilon \quad \text{for all anticyclones} \quad \text{(B7)}$$

which thus travel westwards faster than the long-wave speed ϵ. For cyclones, ($h \leqslant 1$),

$$X_t = -\epsilon(-E)/(-M)$$

where

$$-E = \iint \left[\frac{1}{2}(1 - h^2) - hv^2\right]dA$$

$$-M = \iint (1 - h)dA > 0. \quad \text{(B8)}$$

Now

$$-E = \iint \left[\frac{1}{2}(1 - h)(1 + h) - hv^2\right]dA$$

$$< \iint [1 - h - hv^2]dA,$$

so that

$$(-E) < (-M)$$

$$X_t > -\epsilon. \quad \text{(B9)}$$

Hence all cyclones propagate either eastward or westward slower than the long-wave speed.

b. *Effects of chain*

Now suppose that each eddy is not quite separate from the next in the chain of eddies. Specifically, suppose the eddy chain repeats cyclically in x with period L. Also suppose that at $x = x_0$ (and $x_0 + L$), the connection between eddies is at its smallest and h contours are oriented east–west, with v zero. Repeating the Ball calculation, but including the contribution at x_0, gives

$$MX_t = \sigma - \epsilon \iint yhudA, \quad \text{(B10)}$$

where

$$\sigma = -L \int h(x_0, y)u(x_0, y)dy. \quad \text{(B11)}$$

We have seen that the second term on the rhs of (B10) is negative (i.e., the anticyclones propagate westward). The first term is also of order ϵ, since u is geostrophic at x_0 to leading order. Multiplying the steady version of (2.2) by h, setting v to zero, and integrating w.r.t. y, gives

$$\sigma \approx \frac{1}{2}\epsilon L \int (h^2(x_0, y) - 1)dy > 0. \quad \text{(B12)}$$

Hence (B10) shows that the effect of a chain of anticyclonic eddies is to retard their westward propagation, as observed in the calculations in section 5.

Rough calculations from Fig. 9 suggest that (B12) is indeed of the right magnitude to account for the change in propagation speed observed. All center-of-mass calculations, however, neglect the flow outside the eddy, so that such formulae should be used with caution.

REFERENCES

Armi, L., and W. Zenk, 1984: Large lenses of highly saline Mediterranean water. *J. Phys. Oceanogr.*, **14**, 1560–1576.

Davey, M. K., and P. D. Killworth, 1984: Isolated waves and eddies in a shallow water model. *J. Phys. Oceanogr.*, **14**, 1047–1064.

Killworth, P. D., 1983: Deep convection in the world ocean. *Rev. Geophys. Space Phys.*, **21**, 1–26.

Kinder, T. H., and Bryden, H., 1987: The 1985–1986 Gibraltar experiment: Data collection and preliminary results. *Eos Trans. Amer. Geophys. Union*, **68**, 791–795.

Longuet-Higgins, M. L., 1965: The response of a stratified ocean to stationary or moving wind systems. *Deep-Sea Res.*, **12**, 923–973.

Luyten, J., and H. Stommel, 1985: Gyres driven by combined wind and buoyancy flux. *J. Phys. Oceanogr.*, **16**, 1551–1560.

Sankey, T., 1973: The formation of deep water in the North-Western Mediterranean. *Progress in Oceanography*, B. Warren, Ed. Pergamon Press, Vol. 6, 159–179.

Talley, L., 1979: Steady two-layer source-sink flow. *Notes on Polar Oceanography*, 1979 Summer Study Program in Geophysical Fluid Dynamics, Woods Hole Oceanographic Institution, M. E. Stern and F. K. Mellor, Eds., 97–118.